MNK Publication

International Journal of Latest Research in Science and Technology **ISSN (Online):2278-5299**
Volume 7, Issue 5: Page No. 21 - 29 , Sep-Oct 2018
https://www.mnkpublication.com/journal/ijlrst/index.php

A DYNAMIC DESIGN ON PORTABLE, LIGHT AND FASTER ALUMINUM-BASED CLIMB-SLIDING INSPECTION ROBOT FOR POWER TRANSMISSION LINE

Ahmad Bala Alhassan[1], Xiaodong Zhang[1,2], Haiming Shen[1] , Jian Guo[1] and Khaled Hamza[1]
[1]School of Mechanical Engineering, Xi'an Jiaotong University, Xi'an 710049, China
[2]Shaanxi Key Laboratory of Intelligent Robot, Xi'an Jiaotong University, Xi'an 710049, China
amadkabo@126.com , xdzhang@xjtu.edu.cn , shenhaiming@stu.xjtu.edu.cn , 1303263182@qq.com

Abstract **: Efficient and uninterrupted transmission of power from generation stations to consumers is crucial for the development of any country. This paper presents the dynamic design on portable, light and faster aluminum-based robot for safe, cost-effective and reliable inspection of power lines. Unlike the existing robots which are slow and heavy, the proposed two arm aluminum 6061 based robot designed using SOLIDWORKS is fast, portable and inexpensive. The designed concept has been actualized into a real lab-scale robot. To investigate the dynamic behavior of the robot, the mechanical properties of the robot were used to represent the system in a mass-spring-damper configuration. The Lagrange's equation was used to derive the mathematical equations of the robot. In addition, MATLAB was utilized for the simulation analysis of the robot under different operating conditions. Finally, a bang-bang input was used to drive the robot along the power line in real-time. The simulations and experimental results show that the designed climb-sliding robot has been successfully implemented and can be used for power line inspection.**

Keywords **–** Lagrange equation; MATLAB simulation; Power transmission line inspection; Service robot; SOLIDWORKS; Vibration analysis

I. INTRODUCTION

The demand for an uninterrupted power supply by industries, government institutions, and the general population has been ever-increasing due to global population growth and technological development. Thus, the need for reliable and efficient inspection of the transmission lines has been a major concern by the power transmission companies. Manual inspection of transmission power lines has been extremely difficult due to the fact that, transmission lines are exposed to harsh weather condition and normally passed across the mountainous area, water bodies and thick forest [1-4].

Power transmission line inspection robots (PTLIRs) are designed to replace the costly, time consuming and unsecured traditional manual inspection techniques that employed the use of human operators. The main purpose of any inspection techniques is to assess the running conditions and detect any potential damage to the transmission lines or its supporting components. At present, researchers focus on two unmanned inspection robots, namely, flying robots and climb-sliding robots [2], [5]. The climbing-sliding robot can climb and slide on the overhead transmission line and autonomously avoid obstacles (towers, clamps, aircraft warning balls) and most importantly inspect the lines. On the one hand, the flying robot uses the flying ability to inspect the lines and its mechanism is more complex as compared to the climbing robot, because it has to be at some distance from the transmission line without touching the transmission line. Thus, this affects the quality of the inspection data recorded.

The major advantage of the flying robot is its ability to avoid obstacle quickly and accurately as compared to the climbing robot that involves a lot of slow maneuvers. Though the climbing robots are simple to design as compared to flying robot, they are not readily available in the market. So, they must be built from scratch before employed in the field, whereas the flying robots are already available in the market which only requires little modification to serve the intended purpose [6-7]. The main advantage of a sliding robot is that it gives detailed and more accurate inspection data as compared to the flying robot.

Over the past couple of years, researchers and research institutes have remarkably focused in the field of robotics, particularly the power line inspection robots. An unmanned autonomous helicopter based smart copter for inspecting power line has been presented in [8]. This robot utilizes the visible light camera and an infrared camera for the line inspection. One of the first climb-sliding inspection robot prototypes designed for transmission lines is presented in [9]. However, this robot has a lot of limitations including a stability problem. However, significant progress has been made for the design of such robots with obstacle avoidance mechanism as presented in [10-12].

In addition, three research institutes were on the front line of the power line inspection revolution. The Tokyo power company's Expliner robot capable of inspecting multiple transmission lines has been proposed in [13-14]. Another advanced robot called Linescout has been designed by Canada hydro-Quebec's research center [15-16]. Also, the

Publication History

Manuscript Received	**:**	**30 October 2018**
Manuscript Accepted	**:**	**7 November 2018**
Revision Received	**:**	**11 November 2018**
Manuscript Published	**:**	**30 November 2018**

American electric power institute's recent developments presented a more portable inspection robot in [17]. This robot is permanently installed on the power line and it sources power from the transmission line. However, it requires modifying the existing power lines by adding extra cables to facilitate the obstacle avoidance mechanism. Thus, this made it a costly inspection approach. Some of the works that focused on the dynamics and simulation of power line inspection robot have been presented in [18-20].

However, the existing PTLIRs are either heavy which made them slow and consumes a lot of energy or have a high running cost, and there are limited mathematical representation and analysis of the robots. In this paper, a portable, light and faster aluminum-based PTLIR is proposed. The designed concept was realized into a lab-scale PTLIR real-time inspection of the power lines. In addition, using the mechanical properties of the robot, the robot was represented as a mass-spring-damper system and therefore modeled using Lagrange's energy equations.

The mechanical parameters of the robot's components basically stiffness and damping coefficient were used for the MATLAB simulation analysis of the robot dynamic behavior. The dynamic response of the robot subjected to step input force, frictional force and white noise wind disturbance were analyzed and investigated. These time domain responses provide comprehensive information about the robot dynamic behavior and also for the selection of suitable control strategies for an efficient and effective operation and control of the climb-sliding PTLIR. The designed has been successfully implemented and tested in a lab environment. The real-time experimental results show that the PTLIR can be used for the power line inspection.

This paper is organized as follows. Section II describes the structural design of the robot including software design and mechanical realization. Section III describes the dynamic behavior and parameter estimation of the robot. Section IV discusses the simulation results. In addition, section IV presented the mechanical set-up and experimental verification of the robot. Finally, section VI presented the conclusion and intended future work.

II. STRUCTURAL DESIGN OF THE ROBOT

A. Conceptual design of the climb-sliding PTLIR

The design concept of this study is illustrated in the flowchart of Fig. 1. Unlike the conventional inspection robots that are sliding or flying, the concept of the proposed robot consists of two detachable robots namely climb-sliding robot and flying robot as shown in Fig. 2(a). The main function of the flying robot (FR) is to convey the sliding robot (SR) to the power transmission line (PTL) and take it back to the ground when the inspection is completed. This makes it easier for placing the robot on or off the line and the climb-sliding robot can autonomously inspect the transmission line and avoid obstacles.

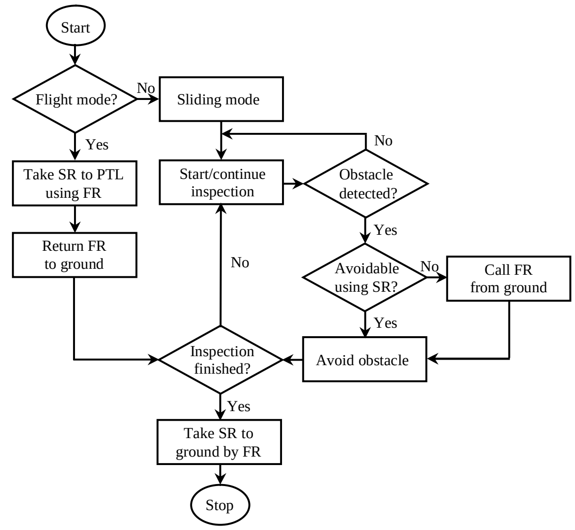

Fig. 1 Work flow chart of flying-climb-sliding inspection robot.

TABLE I
DIMENSION OF THE DESIGNED ROBOT PARTS

S/N	Item	Length	Base	Thickness	Diameter
1	gripper	177mm	150mm	3mm	-
2	circular pipe	400mm	-	3mm	20mm
3	Robot trunk	450mm	60mm	3mm	-

In a situation where the obstacle is too big (e.g tower), the flying robot will be reattached to the climb-sliding robot to avoid the obstacle. The complete robot has a rectangular shape and the dimensions of the individual components are tabulated in Table 1.

However, at this point, we focused on the climb-sliding robot which needs to be designed from scratch. The two-arm climb-sliding robot has two isosceles triangular grippers, two circular pipes arm and a rectangular base which housed the root's electronics and power supply unit as shown in Fig. 2(b). For motion control, the robot basically consists of six motors; two for the rollers for motion along the line and four for the manipulation of the arms during obstacle avoidance mechanism. Two additional rollers and one safety lock are attached to each gripper for support and smooth motion of the robot especially when the transmission cable sagged or slanted. In addition, a steering engine is installed for navigation and guidance as shown in Fig. 2 (c).

An example of an obstacle avoidance procedure is illustrated in Fig. 3 (a-i) for an airplane warning ball. Initially, when the robot senses an obstacle, the robot unlocks the safety lock of the front roller and use the adjustment motors to open the robot arm to avoid the obstacle as shown in (a-d). The front adjustment motors will then take the roller back and closes the lock. In a similar passion, the rear roller will now open as in (e-f), and the rear adjustment motor will rotate the arm away from the power cable until the obstacle is avoided as in (g). The arm will then be rotated back to the power cable as shown in (h). Finally, the lock will be closed and the robot can continue its motion as shown in (i)

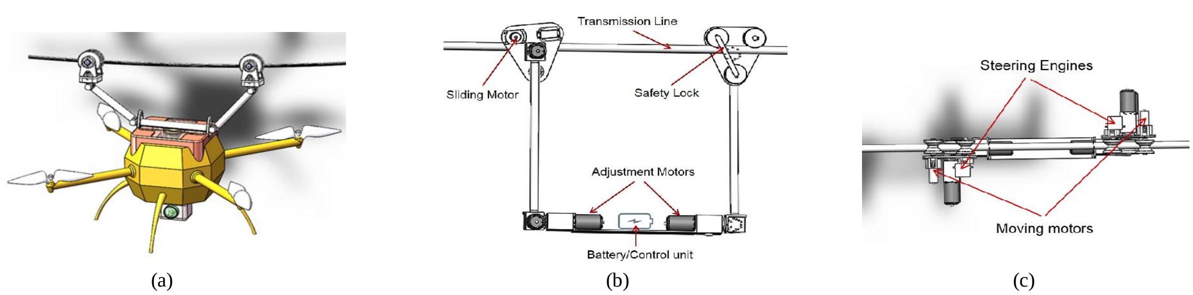

(b) Fig. 2 Structure of the integrated PTLIR: (a) Flying-climb-sliding (b) climb-sliding only (c) rollers and steering engines positions.

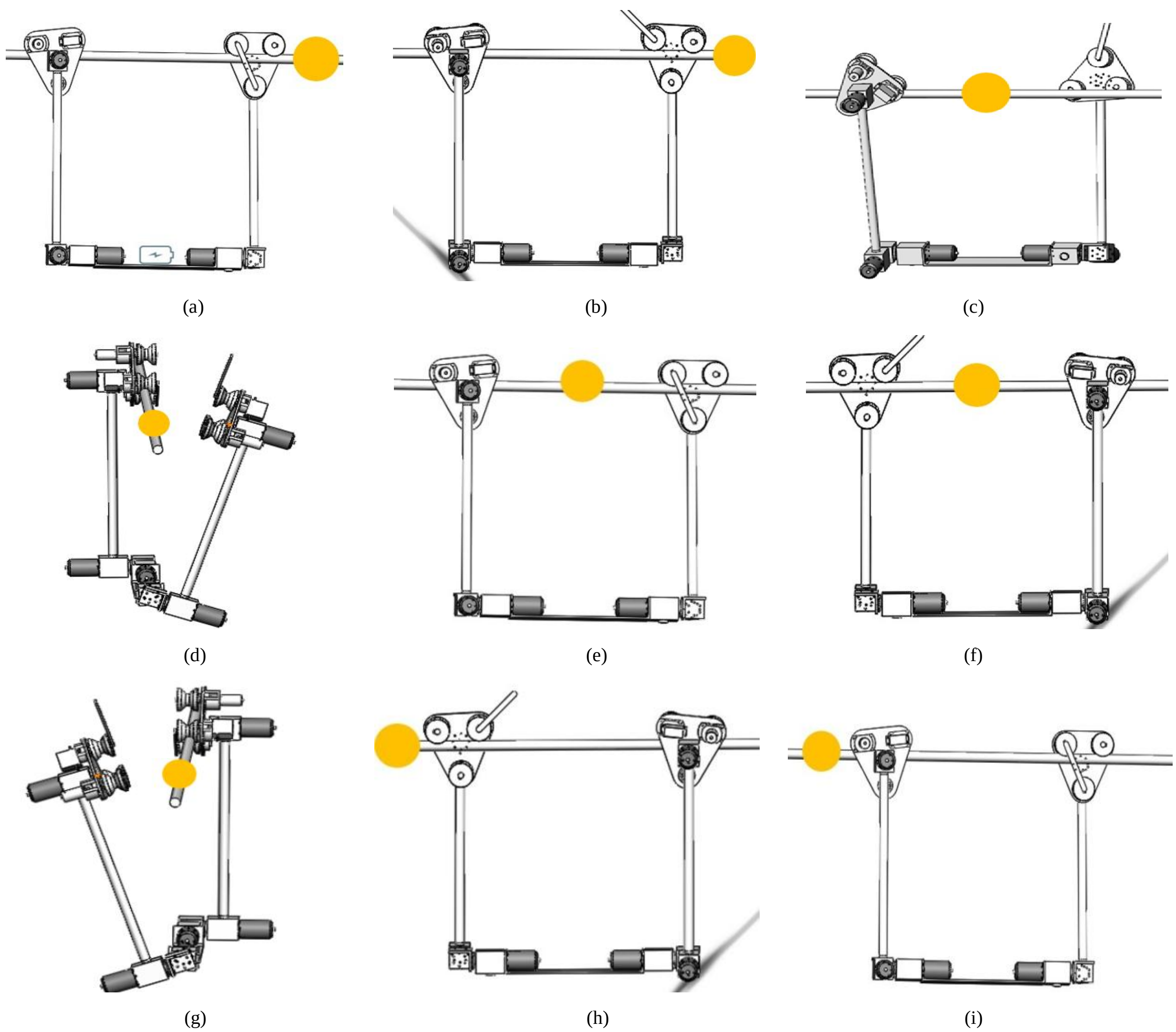

Fig. 3 Typical procedures from (a) to (i) for an airplane warning ball obstacle avoidance along the transmission line.

B. Design of BLDC motors for the climb-sliding PTLIR

This section presents the types of motors selected for the motion control of this PTLIR. The robot can be powered by an external power source (24V battery) and the supporting circuitries like the motor driver were housed on the robot base. Furthermore, a highly efficient Robomaster brushless DC motor was chosen for the robot motion and rotation. An RM2006 P36 BLDC was installed for each of the two rollers and an RM3508 P19 BLDC was chosen for each of the four joints for manipulations. These motors were selected due to their proven high dynamic response, high efficiency, wide speed ranges, and low maintenance. Also, the motors were controlled by C620 speed controller as prescribed by the manufacturer. The summary of the motors' characteristics are given by the manufacturer's data sheet as shown in Table 2 [21].

TABLE II
SELECTED BLDC MOTOR PARAMETERS

S/N	Parameter	M3508 P19	M2006 P36
1	rotational speed (without payload)	482 rpm	500 rpm
2	current (without payload)	0.78 A	0.6 A
3	rated rotational Speed	469 rpm	416 rpm
4	rated torque (continuous torque)	3 N·m	1 N·m
5	rated current	10 A	3 A

III. Dynamic modelling and parameter estimation of the climb-sliding PTLIR

The derivation of the mathematical model of an inspection line robot is very complex due to its higher number of degree of freedom and the associated nonlinearities. However, this study proposes a new method to model the robot in a mass-spring-damper configuration based on the fact that, a continuous system theoretically having infinite number of degree of freedom can be approximated into a single degree of freedom mass-spring-damper, if the dominant mode can be isolated. That is to say that with known system parameters (damping coefficient and stiffness), the robot can be model and analyze.

A. Dynamic modelling

The vertical components of the robots (arm and gripper) are considered to undergo axial tension when the robot moves along the power line. The proposed schematic diagram of the robot is shown in Fig. 4, where $\delta_{1,}$ $\delta_{2,}$ ($\delta_{3,}$ $\delta_{4,}$ δ_5) are the displacements of rear arm of mass m_1, a front arm of mass m_2 and robot base of mass M respectively in the *y*-direction. F_1 and f_2, f_{r1} and f_{r2}, f_w are the actuator force, frictional force and wind disturbance respectively. Also, γ_1 and γ_2 are the input disturbances when the robot immediately lands (climb) on the power line, λ_1 and λ_2 are the distance between the center of the robot to the left and right edges of the robot, respectively.

In addition, c_1, k_1 and c_2, k_2 are the damping coefficient, stiffness of the rear and front triangular gripper of the robot, respectively. c_3, k_3 and c_4, k_4 are the damping coefficient, stiffness of the rear and front circular arm of the robot, respectively. Finally, β is the angular displacement of the base of the robot and the robot base has a moment of inertia, J for the rotation about the centre of mass given in [22], as expressed in Eq. (1).

$$J = \frac{M(\lambda_1 + \lambda_2)}{12} \tag{1}$$

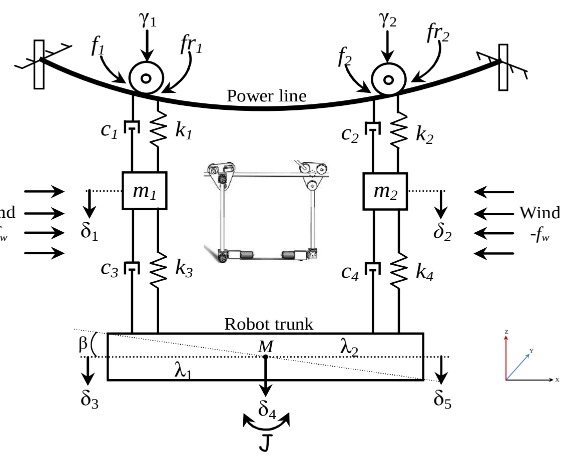

Fig. 4 Mass-spring-damper schematic diagram of the PTLIR.

Moreover, All Aluminum Alloy (AAA) which is one of the most common power transmission cables is considered in this study and while the robot is made from aluminum 6061, the coupling force between the robot and the power cable is the frictional force. Thus, the climb-sliding robot will experience undesirable vibrations during two operating scenarios;

(i) Climb operation: This operation resulted when the robot grasped the power line and thus, the robot will vibrate due to vertical displacements (γ_1 and γ_2) caused by the combined mass of the robot (m_1+m_2+M) and the gravitational acceleration (g).

(ii) Sliding operation: After the robot grasped and landed on the line, the robot then slides along the line using two rollers powered by the actuator force (f_1 and f_2). However, the motion could be affected by two factors; wind disturbance which can be in same or opposite direction of motion of the robot ($\pm fw$) and the kinetic friction (μN) where N is the normal force and μ is the friction coefficient.

The Lagrange Equation given in [19] was used for deriving the mathematical equations of the robot as expressed in Eq. (2).

$$\frac{d}{dt}\left(\frac{dT}{d\dot{q}_i}\right) - \frac{dT}{dq_i} + \frac{dU}{dq_i} = Q_i \quad ; \quad i = 1, 2, 3 \ldots n \tag{2}$$

where q_i is the independent generalized coordinate, Q_i is the total non-conservative generalized forces including external forces, frictional forces and damping forces, and T is the kinetic energy of the system with n coordinate points given in Eq. (3).

$$T = \sum_{i=1}^{n} \frac{1}{2} m_i \dot{q}_i^2 \tag{3}$$

and U is the potential energy consisting of energies due to gravity and elastic potential as given in Eq. (4).

$$U = \sum_{i=1}^{n} \left(\frac{1}{2} k_i q_i^2 + m_i g h_i \right) \tag{4}$$

where h is the height from mass center to a reference point. The total kinetic and potential energies of the robot are given in Eqs. (5) and (6) respectively.

$$T = \frac{1}{2} m_1 \dot{\delta}_1^2 + \frac{1}{2} m_2 \dot{\delta}_2^2 + \frac{1}{2} M \dot{\delta}_4^2 + \frac{1}{2} J \dot{\beta}^2 \tag{5}$$

$$\begin{aligned} U = & \frac{1}{2}\left(k_1(\delta_1 - \gamma_1)^2 + k_2(\delta_2 - \gamma_2)^2 + k_3(\delta_3 - \delta_1)^2 \right) \\ & + \frac{1}{2} k_4 (\delta_5 - \delta_2)^2 - m_1 g \delta_1 - m_2 g \delta_2 - M g \delta_4 \end{aligned} \tag{6}$$

In addition, at equilibrium, $\delta_3 = \delta_4 = \delta_5$, however in the presence of external excitation, δ_3 and δ_5 changes as shown in Eq. (7).

$$\delta_3 = \delta_4 - \lambda_1 \beta \quad ; \quad \delta_5 = \delta_4 + \lambda_2 \beta \tag{7}$$

Thus, for the four coordinates points, i.e $q_1=\delta_1$, $q_2=\delta_2$, $q_3=\delta_4$ and $q_4=\beta$, the terms of Eq. (2) can be calculated. Hence, solving for Eq. (2) for all the four coordinates yields the second order dynamic equations for m_1, m_2, M and J of the complete robot respectively as expressed in Eq. (11) - (14).

$$\begin{aligned} & m_1 \ddot{\delta}_1(t) + (k_1 + k_3)\delta_1(t) + (c_1 + c_3)\dot{\delta}_1(t) - k_1 \gamma_1(t) \\ & - c_1 \dot{\gamma}_1(t) - k_3 \delta_4(t) - c_3 \dot{\delta}_4(t) + \lambda_1 k_3 \beta(t) \\ & + \lambda_1 c_3 \dot{\beta}(t) = f_1 - f_{r1} \pm f_w + m_1 g \end{aligned} \tag{11}$$

$$\begin{aligned} & m_2 \ddot{\delta}_2(t) + (k_2 + k_4)\delta_2(t) + (c_2 + c_4)\dot{\delta}_2(t) \\ & - k_2 \gamma_2(t) \quad - c_2 \dot{\gamma}_2(t) - k_4 \delta_4(t) - c_4 \dot{\delta}_4(t) \\ & - \lambda_2 k_4 \beta(t) + \lambda_2 c_4 \dot{\beta}(t) = f_2 - f_2 \pm f_w + m_2 g \end{aligned} \tag{12}$$

$$\begin{aligned} & M \ddot{\delta}_4(t) + (k_3 + k_4)\delta_4(t) + (c_3 + c_4)\dot{\delta}_4(t) - k_3 \delta_1(t) \\ & - c_3 \dot{\delta}_1(t) - k_4 \delta_2(t) - c_4 \dot{\delta}_2(t) - (\lambda_1 k_3 - \lambda_2 k_4)\beta(t) \\ & - (\lambda_1 c_3 - \lambda_2 c_4)\dot{\beta}(t) = f_1 - f_{r1} + f_2 - f_{r2} \\ & \pm f_w + Mg \end{aligned} \tag{13}$$

$$\begin{aligned} & J \ddot{\beta}(t) + (\lambda_1^2 k_3 + \lambda_2^2 k_4)\beta(t) + (\lambda_1^2 c_3 + \lambda_2^2 c_4)\dot{\beta}(t) \\ & - (\lambda_1 k_3 - \lambda_2 k_4)\delta_4(t) - (\lambda_1 c_3 + \lambda_1 c_4)\dot{\delta}_4(t) \\ & - \lambda_2 k_4 \delta_2(t) - \lambda_2 c_4 \dot{\delta}_2(t) + \lambda_1 k_3 \delta_1(t) \\ & + \lambda_1 c_3 \dot{\delta}_1(t) = -\lambda_1 (f_1 - f_{r1}) + \lambda_2 (f_2 - f_{r2}) \end{aligned} \tag{14}$$

However, it can be noted that one of the forcing functions (γ_1 and γ_2) have a derivative term and the state variable must be chosen such that the resulting state equations has no derivative of the input function [23]. Thus, after selecting appropriate state variables, the robot dynamics of Eq. (11)-(14) are represented in the standard state space representation of Eq. (15) in Eq. (16), where A, B and C is the system matrix, input matrix and output matrix respectively. On the other hand, the main of objective of this study is to analysis the behavior of the robot base and the angular displacement when the robot moves along the power line and or in the presence of wind disturbance. Thus, the robot base linear displacement ($\delta 4$) and its angular displacement (β) are considered the output of the system (y_{out}), where $c_{ij}=c_i+c_j$ and $k_{ij}=k_i+k_j$; i and j are positive integers.

$$\begin{cases} \dot{x}(t) = Ax(t) + Bu(t) \\ y(t) = Cx(t) \end{cases} \tag{15}$$

$$\begin{bmatrix} \dot{\delta}_1 \\ \ddot{\delta}_1 \\ \dot{\delta}_2 \\ \ddot{\delta}_2 \\ \dot{\delta}_4 \\ \ddot{\delta}_4 \\ \dot{\beta} \\ \ddot{\beta} \end{bmatrix} = \begin{bmatrix} 0 & 1 & 0 & 0 & 0 & 0 & 0 & 0 \\ -\frac{k_{13}}{m_1} & -\frac{c_{13}}{m_1} & 0 & 0 & \frac{k_3}{m_1} & \frac{c_3}{m_1} & -\frac{\lambda_1 k_3}{m_1} & -\frac{\lambda_1 c_3}{m_1} \\ 0 & 0 & 0 & 1 & 0 & 0 & 0 & 0 \\ 0 & 0 & -\frac{k_{24}}{m_2} & -\frac{c_{24}}{m_2} & \frac{k_4}{m_2} & \frac{c_4}{m_2} & \frac{\lambda_2 k_4}{m_2} & \frac{\lambda_2 c_4}{m_2} \\ 0 & 0 & 0 & 0 & 0 & 1 & 0 & 0 \\ \frac{k_3}{M} & \frac{c_3}{M} & \frac{k_4}{M} & \frac{c_4}{M} & -\frac{k_{34}}{M} & -\frac{c_{34}}{M} & \frac{\lambda_1 k_3 - \lambda_2 k_4}{M} & \frac{\lambda_1 c_3 - \lambda_2 c_4}{M} \\ 0 & 0 & 0 & 0 & 0 & 0 & 0 & 1 \\ \frac{-\lambda_1 k_3}{J} & \frac{-\lambda_1 c_3}{J} & \frac{\lambda_2 k_4}{J} & \frac{\lambda_2 c_4}{J} & \frac{\lambda_1 k_3 - \lambda_2 k_4}{J} & \frac{\lambda_1 c_3 - \lambda_2 c_4}{J} & \frac{-\lambda_1^2 k_3 + \lambda_2^2 k_4}{J} & \frac{-\lambda_1^2 c_3 + \lambda_2^2 c_4}{J} \end{bmatrix} \begin{bmatrix} \delta_1 \\ \dot{\delta}_1 \\ \delta_2 \\ \dot{\delta}_2 \\ \delta_4 \\ \dot{\delta}_4 \\ \beta \\ \dot{\beta} \end{bmatrix}$$

$$+ \begin{bmatrix} 0 & 0 \\ \frac{1}{m1} & 0 \\ 0 & 0 \\ 0 & \frac{1}{m2} \\ 0 & 0 \\ \frac{1}{M} & \frac{1}{M} \\ 0 & 0 \\ \frac{-\lambda_1}{J} & \frac{\lambda_2}{J} \end{bmatrix} \begin{bmatrix} f_1 - f_{r1} \\ f_2 - f_{r2} \end{bmatrix} + \begin{bmatrix} 0 \\ 1 \\ 0 \\ 1 \\ 0 \\ 1 \\ 0 \\ 0 \end{bmatrix} g + \begin{bmatrix} \frac{c1}{m1} & 0 \\ \frac{k1}{m1} - \frac{(c13)c1}{(m1)^2} & 0 \\ 0 & \frac{c2}{m2} \\ 0 & \frac{k2}{m2} - \frac{(c24)c2}{(m2)^2} \\ 0 & 0 \\ \frac{c1c3}{m1M} & \frac{c2c4}{m2M} \\ 0 & 0 \\ \frac{-\lambda_1 c1c3}{m1J} & \frac{\lambda_2 c2c4}{m2J} \end{bmatrix} \begin{bmatrix} \gamma_1 \\ \gamma_2 \end{bmatrix} \pm \begin{bmatrix} 0 \\ \frac{1}{m1} \\ 0 \\ \frac{1}{m2} \\ 0 \\ \frac{1}{M} \\ 0 \\ 0 \end{bmatrix} f_w \tag{16}$$

$$y_{Out} = \begin{bmatrix} 0 & 0 & 0 & 0 & 1 & 0 & 0 & 0 \\ 0 & 0 & 0 & 0 & 0 & 0 & 1 & 0 \end{bmatrix} \begin{bmatrix} \delta_1 & \dot{\delta}_1 & \delta_2 & \dot{\delta}_2 & \delta_4 & \dot{\delta}_4 & \beta & \dot{\beta} \end{bmatrix}^T$$

B. Parameter Estimation

The required parameters for the analysis are the damping coefficient (c) and stiffness (k). However, if one parameter is identified, the other can be analytically calculated using mathematical relations and the most common method for mechanical modal identification is the impact hammer test. The test uses a specialized hammer to impact a known force at different points on the structure and the corresponding vibratory responses are recorded using an accelerometer. Frequency response function (FRF) is normally used to analyze the recorded data for the parameters identification. This experiment was conducted on a similar aluminum material and a damping ratio of 0.35% was obtained as comprehensively presented in [24].

In addition, the Young modulus which describes the characteristics of the constituent element has a constant value and its value for aluminum 6061 is 68.9GPa [25]. The coefficient of friction for aluminum rolling on the aluminum metal of 0.34 was adopted in this work as determined in [26]. Also, the expression of stiffness for a solid shape under tension or compression and the damping coefficient is respectively given in [22] as expressed in Eqs. (17)-(18).

$$k = \frac{AE}{L} \tag{17}$$

$$c = 2\zeta\sqrt{km} \tag{18}$$

where A is the cross-sectional area, E is the Young's Modulus, L is the length of the element, ζ is the damping ratio and m is the mass of the element. With the known area of the robot components, the parameters used in this study were estimated as illustrated in Table 3.

TABLE III
PARAMETERS FOR SIMULTAION

$\lambda_1 = 0.20$ m	$\lambda_2 = 0.25$ m
$m_1 = m_2 = 0.50$ kg	M = 2.0 kg
$k_1 = k_2 = 4.68E09$ N/m	$c_1 = c_2 = 478.90$ Ns/m
$k_3 = k_4 = 5.41E07$ N/m	$c_3 = c_4 = 36.41$ Ns/m

IV. DYNAMIC SIMULATIONS AND RESULT

In this section, MATLAB simulation results of the derived dynamic equations are presented and analyzed. The objective of these analyses is to study the dynamic behavior of the proposed robot during climbing and sliding operations under the influence of friction and external wind disturbance. As stated earlier, the study focused on the robot base vertical displacement (δ4) and the corresponding angular displacement (β) which describes the dynamic vibrations of the robot during power line inspections. The desired response is to have a smooth motion of the robot without vibrations. However, numerical values of the parameters of the robot are required for the simulations and thus, parameters of Table 3 were used for the simulation of Eq. (16).

To analysis the response of the system during climbing operation i.e when the robot just landed on the power line, a pulse input signal is used to represent the contact force that causes the robot to vibrate. Fig. 5(a) shows the response of the robot displacement, it can be seen that with a reference pulse signal representing a sudden 10mm vertical displacement of the power line for two seconds cause the robot to vibrate to a maximum value of 20mm before settling within zero. Fig. 5(b) shows the response of the angular displacement when the center of mass is assumed to be at the center of the robot. At this point, λ1=λ2=225mm, which technically means that the robot is well balanced and there would be no angular displacement, 2.8E-21 in this case. In reality, the equilibrium state and thus, the center of mass of the robot can either be slanted to left or right which increases the displacement. Hence, Fig. 6(a) shows the response of the angular displacement for the tabulated parameters (λ1=200mm and λ2=250mm) shows an increased displacement reaching a maximum value of 1.534E-05rad and settled at zero. The displacements are faster at two points; the time of impact and immediately when the impact is removed before finally settled at zero.

In addition, to investigate the behavior of the robot, a step input is used as the driving force of the sliding motors and a dynamic friction is added to the contact between the rollers and the power line cable for more realistic analysis. Fig. 6(b) and Fig. 7(a) show the response of the linear displacement and angular displacement of the robot using the sliding motors, respectively. By assuming a frictionless surface in a situation where rain lubricated the transmission cable, the friction coefficient is set to zero and the response shows an increased linear and angular vertical displacements of the robot. This is due to the fact that, the sliding motors move faster and hence, generates more vibrations in the absence of friction.

Moreover, a random white noise representing a wind disturbance shown in Fig. 7(b) is added to the system in two directions. The responses of the positive wind in the direction of motion and that of the negative wind opposing the motion of the robot are respectively shown in Fig. 8(a) and Fig. 8(b). The result shows that in each case wind disturbance increases the vibration of the robots.

In summary, the maximum absolute linear and angular displacements for all the presented cases are illustrated in Fig. 9(a) and Fig. 9(b), respectively. It can be observed that with the 10mm reference vertical displacement, an 11% increase of the displacement was recorded when the robot climbs the power line as compared to normal sliding movement. However, increasing the aggressiveness of the grasping (climbing) from 10mm will increase the corresponding vertical vibrations. Moreover, 5% and 120% increase in displacement was recorded for frictionless and wind disturbances respectively as compared to the normal sliding operation of magnitude 0.018m as shown in Fig. 9(a). Likewise, the angular displacement of magnitude 1.22E-5rad increases by 2% for frictionless motion, 25% for climbing and 85% for wind disturbances as shown in Fig 9(b). In this case, we can observe that the angular displacement is very small and hence, it is clear that the angular vibration of the robot is insignificant.

Finally, these values may change when the input perturbations changes, however, the nature or pattern of the responses will remain the same. Thus, these time domain analyses provide an insight into the dynamic behavior of the robot under certain conditions and demonstrated that the robot has fast time response and good vibration settling time and hence, would be suitable for power line inspections.

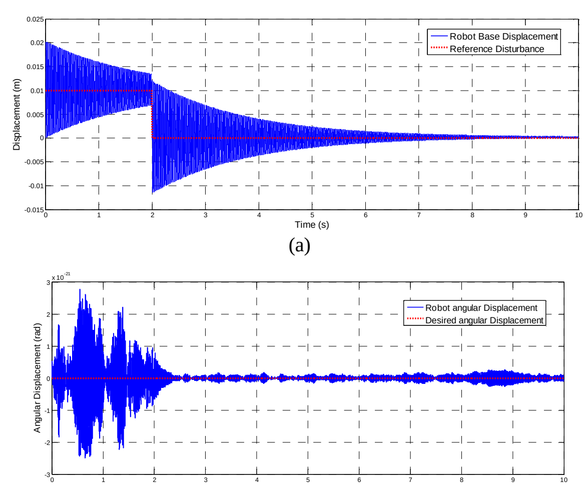

(a)

(b)

Fig. 5 Climbing operation: (a) Linear displacement; (b) angular displacement for $\lambda_1 = \lambda_2 = 225$mm.

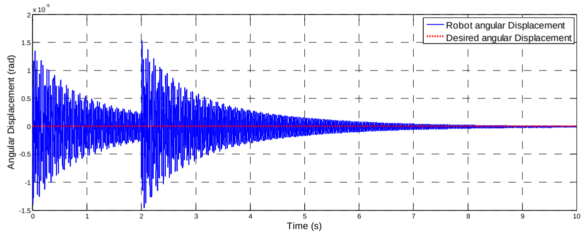

(a)

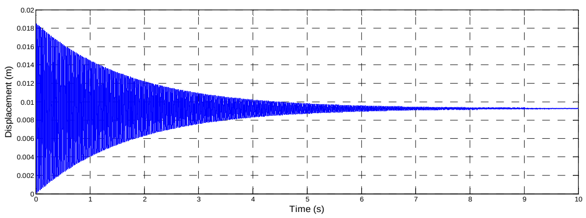

(b)

Fig. 6 Angular displacement for climbing operation for $\lambda_1 \neq \lambda_2$; (b) linear displacement for the sliding motions.

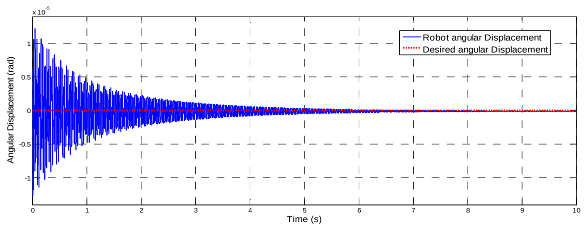

(a)

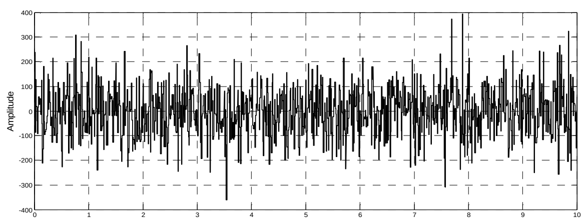

(b)

Fig. 7 Angular displacement for the sliding motions; (b) white noise wind disturbance.

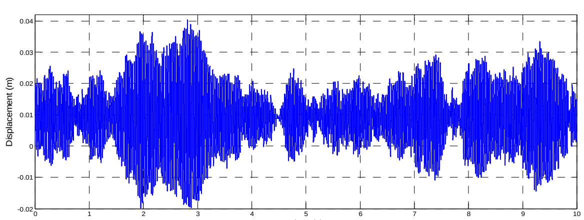

(a)

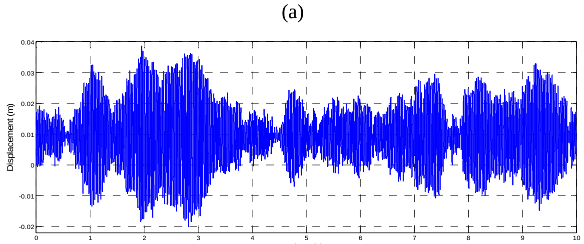

(b)

Fig. 8 Linear displacement: (a) Positive wind disturbance; (b) negative wind disturbance.

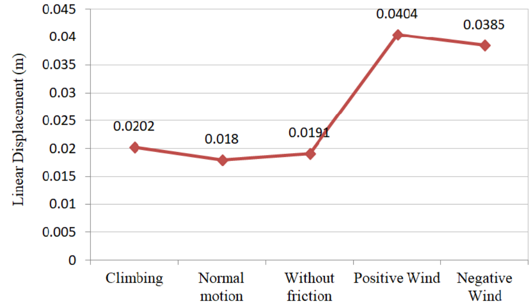

(a)

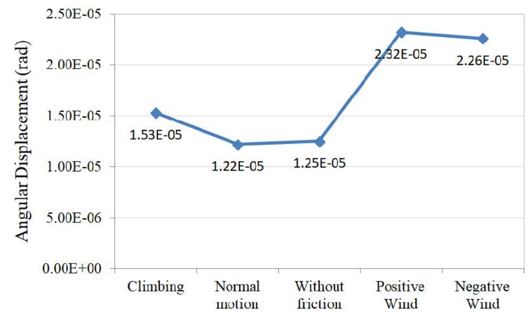

(b)

Fig. 9 Summary of displacements: (a) linear displacement; (b) angular displacement.

V. Experimental Set-up and Results

The experimental study was conducted in order to verify the effectiveness of the designed robot. The designed PTLIR has been realized into a real lab scale robot as shown in Fig. 10. The 0.5m by 0.6m robot is light and portable as it only weighs 7.5Kg including the electronics circuits. As stated earlier, one of the most commonly used transmission cable; the all aluminum alloy (AAA) conductor was employed in this study due to its strength to noise mass ratio, high resistance to corrosion and good sag characteristics [27]. However, the structure was tested in a lab environment; thus, the cable length was limited to 3m and supported by 0.8m high fixed towers. A tri-axis ADXL335 accelerometer was chosen and installed on the robot base for the induced vibration measurements of the structure due to its cost-effectiveness and low power consumption (0.35mA) [28]. Unlike the simulation analysis that covers the vertical vibration of the robot, this accelerometer allowed us to analyze the vibration in 3-axis. In addition, the simulation results highlighted the response of the robot without control. However, for safety concerns, the robot cannot be tested without motor controller. Thus, a C620 speed controller was installed to the driving motors as prescribed by the motor manufacture as previously described in section II (B). Arduino Uno microcontroller was used as the data acquisition system and the real-time vibratory response of the structure was recorded and analyzed using MATLAB as shown on the monitoring PC.

To demonstrate the effectiveness of the designed PTLIR, the two axes (x and y) responses during start-up (on) and braking (off) conditions were analyzed. Fig. 11(a) shows the reference bang-bang voltage signal used to drive the robot along the power cable. The bang-bang signal drives the robot forward (+24V) and backward (-24V) for 5 seconds each for

6 minutes such that its dynamic behavior on the transmission line can be adequately studied in real-time. The vibrations in x, y and z-axes are shown in Fig. 11(b), Fig. 12(a) and Fig. 12(b), respectively. Furthermore, the test was under the influence of external disturbance and inherent electronic noises, the maximum vibration of x, y and z-axes is 0.169m/s2, 0.105m/s2 and 0.37m/s2, respectively. This shows that the vertical vibration in the z-axis is higher than the horizontal vibrations in x and y directions as previously assumed during modeling. However, based on the general vibration severity graph [29], 0.169m/s2 is an extremely smooth vibration and thus, the experiment demonstrated that the robot can slide along the power cable without much vibration as desired.

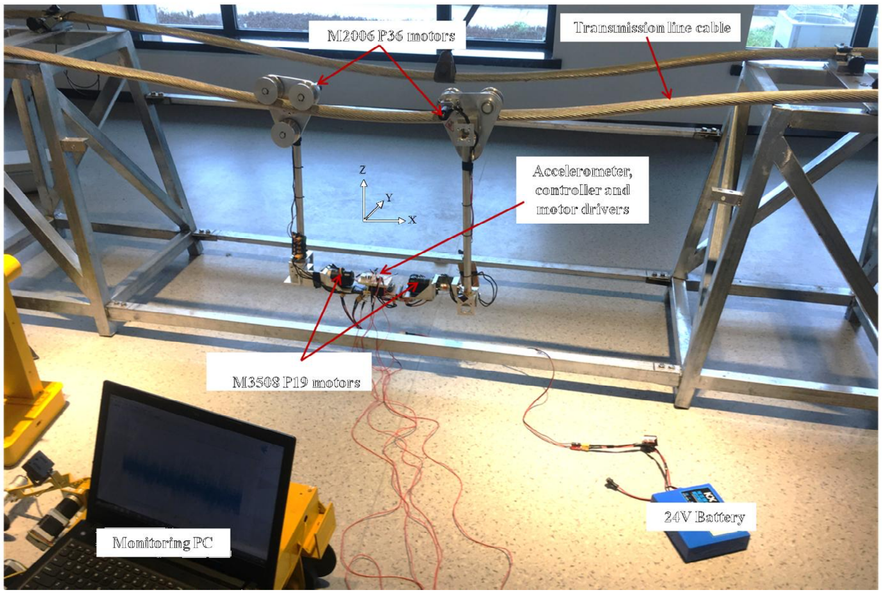

Fig. 10 The lab scale PTLIR experimental set-up.

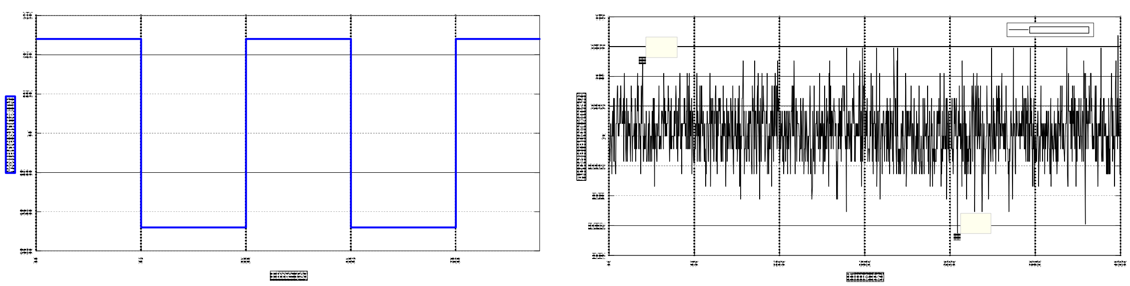

(a) (b)

Fig. 11 (a) Reference bang-bang input signal; (b) output vibration of the PTLIR in x-axis.

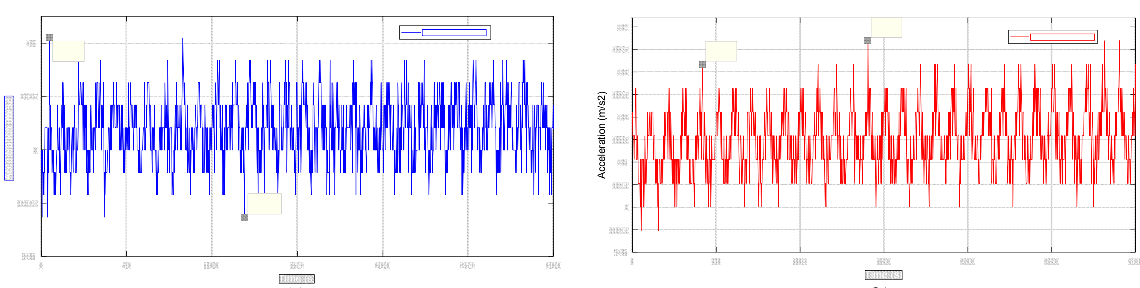

(a) (b)

Fig. 12 (a) Output vibration of the PTLIR in y-axis; (b) output vibration of the PTLIR in z-axis.

VI. Conclusions

The existing power line inspection robots were large and heavy which made them slow and consumes a lot of energy. This work is part of the project under the state key lab of intelligent robotics of Xi'an Jiaotong University, China to design an integrated fast and portable fly-climb-sliding robot for an efficient power line inspection. The climb-sliding structure was initially designed using SOLIDWORKS and later realized into an aluminum 6061 based lab-scale power line inspection robot. Furthermore, using the mechanical properties of the structure, the system was represented into an equivalent mass-spring-damper configuration. The Lagrangian energy equation was used to derive the dynamic equations of the robot. MATLAB simulation was used to study the dynamic responses of the robot under different perturbations including pulse input force, friction force and white noise wind disturbance. The simulation and real-time experimental results of the robot sliding along the transmission line demonstrated that the robot has a good time response with small induced vibration. These results provide comprehensive information about the dynamic behavior of the robot and confirmed that the robot is cost effective and suitable for an autonomous power transmission line inspection. Thus, our future work comprises of designing an intelligent control for the obstacle avoidance mechanism and an installation of sensing and imaging equipment on the robot for real-time inspection of the transmission line and its components.

ACKNOWLEDGMENT

The authors are grateful for the support provided by the Key research and development plan of Shaanxi Province, China (2017ZDXM-G-9-2).

REFERENCES

[1] Y. G. Wang, H. D. Yu, and J. K. Xu, "Design and simulation on inspection robot for high-voltage transmission lines," *Appl. Mech. Mater.*, vol. 615, pp. 173–180, 2014.

[2] M. Nayyerloo, X. Chen, W. Wang, and J. Chase, "Cable-Climbing Robots for Power Transmission Lines Inspection," *Mob. Robot. – State Art Land, Sea, Air, Collab. Mission.*, pp. 63–84, 2009.

[3] Z. Li and Y. Ruan, "Autonomous inspection robot for power transmission lines maintenance while operating on the overhead ground wires," *Int. J. Adv. Robot. Syst.*, vol. 7, no. 4, pp. 107–112, 2010.

[4] L. G. García-valdovinos, A. Velarde-sánchez, L. Llano-vizcaya, T. Salgado-, F. Hernández-rosales, and F. Martínez-soto, "Dynamic Model and Simulation of an Inspection Robot for Power Transmission Lines : Preliminary Results," *Int. Conf. Appl. Robot. Power Ind.*, pp. 1–6, 2010.

[5] R. S. Gonçalves and J. C. M. Carvalho, "A mobile robot to be applied in high-voltage power lines," *J. Brazilian Soc. Mech. Sci. Eng.*, vol. 37, no. 1, pp. 349–359, 2014.

[6] S. N. D. Coe, R. C. Yeola, and S. Phule, "A REVIEW OF INSPECTION OF HVDC TRANSMISSION LINE BY USING ROBOT," *Int. J. Adv. Res. Innov. Ideas Educ.*, vol. 3, pp. 1848–1854, 2017.

[7] K. H. Seok and Y. S. Kim, "A state of the art of power transmission line maintenance robots," *J. Electr. Eng. Technol.*, vol. 11, no. 5, pp. 1412–1422, 2016.

[8] B. Wang, X. Chen, Q. Wang, L. Liu, H. Zhang, and B. Li, "Power line inspection with a flying robot," *2010 1st Int. Conf. Appl. Robot. Power Ind. CARPI 2010*, pp. 1–6, 2010.

[9] J. Sawada, K. Kusumoto, Y. Maikawa, T. Munakata, and Y. Ishikawa, "A mobile robot for inspection of power transmission lines," *IEEE Trans. Power Deliv.*, vol. 6, no. 1, pp. 309–315, 1991.

[10] S. Y. Fu, Z. G. Hou, Z. Z. Liang, M. Tan, F. S. Jing, Q. Zuo, and Y. C. Zhang, "Image-based visual servoing for power transmission line inspection robot," *Int. J. Model. Identif. Control*, vol. 6, no. 3, p. 239, 2009.

[11] G. Wu, X. Xu, H. Xiao, J. Dai, X. Xiao, Z. Huang, and L. Ruan, "A novel self-navigated inspection robot along high-voltage power transmission line and its application," *Lect. Notes Comput. Sci. (including Subser. Lect. Notes Artif. Intell. Lect. Notes Bioinformatics)*, vol. 5315, no. PART 2, pp. 1145–1154, 2008.

[12] Z. Bin Ren, R. Yi, L. Zheng, and Y. Yong, "Motion planning of inspection robot suspended on overhead ground wires for obstacle-navigation," *2009 Chinese Control Decis. Conf. CCDC 2009*, pp. 1322–1326, 2009.

[13] P. Debenest, M. Guarnieri, K. Takita, E. F. Fukushima, S. Hirose, K. Tamura, A. Kimura, H. Kubokawa, N. Iwama, and F. Shiga, "Expliner - Robot for inspection of transmission lines," *Proc. - IEEE Int. Conf. Robot. Autom.*, pp. 3978–3984, 2008.

[14] P. Debenest and M. Guarnieri, "Expliner - From prototype towards a practical robot for inspection of high-voltage lines," *2010 1st Int. Conf. Appl. Robot. Power Ind. CARPI 2010*, pp. 1–6, 2010.

[15] N. Pouliot, P. Latulippe, and S. Montambault, "Reliable and intuitive teleoperation of LineScout: A mobile robot for live transmission line maintenance," *2009 IEEE/RSJ Int. Conf. Intell. Robot. Syst. IROS 2009*, pp. 1703–1710, 2009.

[16] N. Pouliot, P. L. Richard, and S. Montambault, "LineScout Technology Opens the Way to Robotic Inspection and Maintenance of High-Voltage Power Lines," *IEEE Power Energy Technol. Syst. J.*, vol. 2, no. 1, pp. 1–11, 2015.

[17] A. Phillips, E. Engdahl, D. McGuire, M. Major, and G. Bartlett, "Autonomous overhead transmission line inspection robot (TI) development and demonstration," *Appl. Robot. Power Ind. (CARPI), 2012 2nd Int. Conf.*, pp. 94–95, 2012.

[18] J. Y. Park, J. K. Lee, B. H. Cho, and K. Y. Oh, "An inspection robot for live-line suspension insulator strings in 345-kV power lines," *IEEE Trans. Power Deliv.*, vol. 27, no. 2, pp. 632–639, 2012.

[19] P. S. D. A. R.C, Narrendar., "Dynamic Modelling and Obstacle Avoidance for Cable Maneuvering Robot In application to Transmission line Inspection robots," *Int. J. Eng. Dev. Res.*, vol. 2, no. 4, pp. 3372–3376, 2014.

[20] X. Xiao, G. Wu, E. Du, and T. Shi, "Dynamic simulation and experimental study of inspection robot for high-voltage transmission-line," *J. Cent. South Univ. Technol.*, vol. 12, no. 6, pp. 726–731, 2005.

[21] (2018) DJ Robomaster website [Online]. Available: https://www.robomaster.com/en-US.

[22] W. T. Thomson, *Theory of Vibrations with Applications*, 5th ed. Santa Barbara, California: Chapman & Hall, 1998.

[23] K. Ogata, "Modern Control Engineering." 5th ed., New York, USA: Prentice Hall, pp. 793–816, 2010.

[24] H. Mevada and D. Patel, "Experimental Determination of Structural Damping of Different Materials," *Procedia Eng.*, vol. 144, pp. 110–115, 2016.

[25] P. Plescia and E. Tempesta, "Analysis of friction coefficients in a vibrating cup mill (ring mill) during grinding," *Tribol. Int.*, vol. 114, pp. 458–468, 2017.

[26] G. Wypych, *Handbook of surface improvement and modification*, First Edit., vol. 1. Toronto: ChemTec Publishing, 2018.

[27] (2018) JYTOP wire and cable website [Online]. Available: https://www.electriccable.cc/Bare-Conductor/All-Aluminum-Alloy-Conductor-AAAC.html

[28] "AXDL335 data sheet," Spartfun Electronics, Norwood, U.S.A.

[29] B. Shannon, "Vibration Measurement Systems and Guidelines for Centrifugal Fans," *AMCA Int. Eng. Conf.*, pp. 4–20, 2008.